

Article

UAV Detection Using Thrust Engine Electromagnetic Spectra

Tomas Jačionis , Vytautas Urbanavičius, Andrius Katkevičius , Vytautas Abromavičius , Artūras Serackis , Tomyslav Sledevič  and Darius Plonis * 

Department of Electronic Systems, Vilnius Gediminas Technical University, Saulėtekio Ave. 11, LT-10223 Vilnius, Lithuania

* Correspondence: darius.plonis@vilniustech.lt

Abstract: Artificial intelligence used in unmanned aerial vehicle (UAV) flight control systems tends to leave UAV control systems without any radio communication emissions, whose signatures in an electromagnetic spectrum (ES) are widely used to detect UAVs. There will be problems in the near future in detecting any dangerous threats associated with UAV swarms, kamikaze unmanned aerial vehicles (UAVs), or any other UAVs with electrically powered thrust engines because of the UAV's flight capabilities in full radio silence mode. This article presents a different approach to the detection of electrically powered multi-rotor UAVs. The main idea is to register the electromagnetic spectrum of the electric thrust engines of the UAV, which varies because of the changing flight conditions. An experiment on a UAV's electric thrust engine-produced electromagnetic spectrum is carried out, presenting the results of the flight-dependent characteristics, which were observed in the electromagnetic spectrum. The electromagnetic signature of the UAV's electric thrust engines is analyzed, discussed, and compared with the most similar behaving electric engine, which was used on the ground as a domestic electric appliance. A precision tunable magnetic antenna is designed, manufactured, and tested in this article. The physical experiments have shown that the ES of the electric thrust engines of multi-rotor UAVs can be detected and recorded for recognition. The unique signatures of the ES of the multi rotor UAV electric engine are recorded and presented as a result of the carried-out experiments. A precision tunable magnetic antenna is evaluated for the reception of the UAV's signature. Moreover, results were obtained during the performed experiments and discussions about the development of the future techniques for the identification of the ES fingerprints of the UAV's electric thrust engine are carried out.

Keywords: electromagnetic signature; electromagnetic spectrum; magnetic antenna; UAV detection



Citation: Jačionis, T.; Urbanavičius, V.; Katkevičius, A.; Abromavičius, V.; Serackis, A.; Sledevič, T.; Plonis, D. UAV Detection Using Thrust Engine Electromagnetic Spectra. *Drones* **2022**, *6*, 306. <https://doi.org/10.3390/drones6100306>

Academic Editor: Andrey V. Savkin

Received: 29 September 2022

Accepted: 17 October 2022

Published: 19 October 2022

Publisher's Note: MDPI stays neutral with regard to jurisdictional claims in published maps and institutional affiliations.



Copyright: © 2022 by the authors. Licensee MDPI, Basel, Switzerland. This article is an open access article distributed under the terms and conditions of the Creative Commons Attribution (CC BY) license (<https://creativecommons.org/licenses/by/4.0/>).

1. Introduction

Unmanned aerial vehicles are rapidly integrating into everyday life by performing previously impossible tasks. The military, academic research, agriculture, and leisure industries are the most active in the development of UAVs. UAVs are equipped with cutting-edge intelligent autonomous technologies aimed at collecting data, conducting search and rescue operations, military missions, firefighting, and medical assistance. Recent developments related to UAV threats have shown that UAVs are capable of conducting targeted, lethal attacks on distant infrastructure and have important global impacts on critical supply [1,2]. On 14 September 2019, a high-volume UAV attack was launched, which reduced Saudi Arabia's oil production by 50% [3]. This year, the Ukrainian–Russian war shows the massive use of UAVs as attack, defense, or intelligence tools [4].

It is important to note the growing danger posed by “kamikaze drones” (a form of UAV loaded with deadly bombs and shrapnel), which are becoming more and more common and lack any effective technological means of detection from terrorist attacks, particularly in densely populated urban areas. These UAVs are typically handcrafted and operate with unique remote controls that are not mass-produced and are easy to find in populated

places [5]. When fully autonomous flight autopilot systems handle flight without the aid of radio communication or navigation, detecting UAVs becomes much more challenging [6].

On 5 August 2018, Venezuelan President N. Maduro was attacked by civilian UAVs, including two DJI M600 UAVs carrying C4 explosives [7]. One of the busiest runways at Gatwick Airport closed on 20 December 2018. Some 110,000 passengers were delayed on 760 flights as UAVs repeatedly flew over the airfield. The threat of drones is clearly one of the biggest unsolved security problems in the near future. As a result, the task of detecting UAVs in no-fly zones becomes a difficult but largely unsolved task [8]. Each country has its own no-fly UAV zones for airport security and strategic infrastructure. However, with the development of intelligent UAV control technology, future high-capacity communication links are likely to fail to achieve the desired security. They are likely to become obsolete.

UAVs that communicate with other devices via radio communication or are controlled by radio communication from other devices could be detected by detecting the radio communication channel. However, UAVs whose control is completely autonomous eliminate this possibility of their detection. For this purpose, alternatives are needed that allow UAVs to be detected in another way.

The article proposes a unique motor-driven antenna that allows the stepless switching of the resonant frequency for signal tracking and reception.

In a recent work, the possibility of detecting drones up to 1.5 m using an extremely low frequency range (5–20 kHz) range was demonstrated [9,10]. Measurement of the magnetic field of the rotating elements of the asynchronous motor and the rotating field of the stator was shown to allow identification of the corresponding frequencies of the motor [11]. The possibility of drone detection using leakage flows from different brushless direct current (BLDC) motors was successfully demonstrated in a low-frequency radio frequency band [12]. A hypothesis has been formulated that, by measuring the spectrum of the engine control signals, we can detect UAV-specific traces in the spectrogram.

1.1. UAV Propulsion Types

In general, propulsion energy is required for takeoff, flight, and landing by all UAVs. All unmanned aerial vehicles (UAVs) except gliders and lighter-than-air devices are propelled during flight by thrust engines. UAVs with glider-type architecture do not require propulsion energy because they can fly using rising air streams, but they do require lifting or towing in the air. UAV engine types based on propulsion energy can be divided into three categories, as shown in (Figure 1).

The propulsion, electric thrust engines are often the best option for recreational UAVs. They can be agile, light, reliable, and easy to handle in flight. However, flight time and distance are limited by batteries. Typically, a gasoline–electric power plant uses a tiny gas engine to extend the range of an unmanned aerial vehicle.

1.2. Types of Engines for UAV's Propulsion

For any UAV to fly, propulsion is a must. An overview of the primary thrust engine types for UAV flight performance is given with an emphasis on internal combustion and electric engines. An internal combustion engine, called a piston, often known as a reciprocating engine, employs one or more reciprocating pistons to transform pressure into rotational motion to generate thrust power from liquid fuel. An electrical device that transforms electrical energy into mechanical energy is known as an electric motor. The interplay of a motor's magnetic field and electric current in its wire windings produces the rotation force of the motor shaft.

An internal combustion engine, known as a two-stroke, completes two cycles in one shaft revolution. In a two-stroke engine, the intake and exhaust processes occur simultaneously at the end of the combustion stroke and at the beginning of the compression stroke. Compared to other forms of internal combustion engines, this type of engine has a high power-to-weight ratio because of the tremendous power that can be achieved in this

way. These engines are fairly lightweight and are frequently utilized for UAV propulsion due to their straightforward construction.

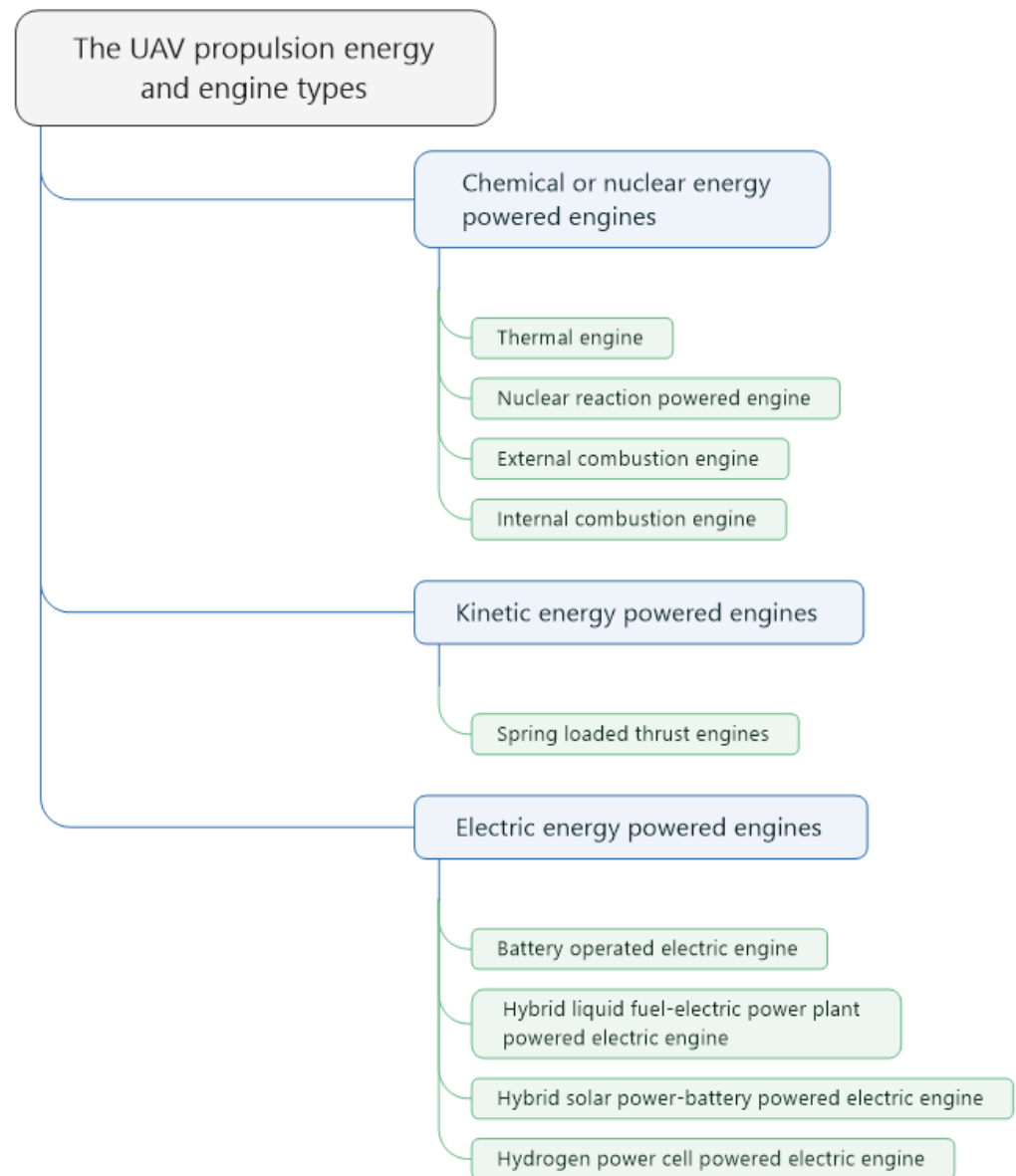


Figure 1. The main UAV propulsion energy and engine types.

A four-stroke engine has a four-stroke duty cycle. They are the intake stroke, compression stroke, power stroke, and exhaust stroke. Four-stroke engines tend to be heavier because they use oil pumps and oil reservoirs to lubricate the engine. The engine has a valve system, which also adds weight. A four-stroke engine provides one power stroke for every two piston cycles (or four piston strokes), resulting in a lower power-to-weight ratio. However, this type of engine is much more reliable and energy efficient than a two-stroke engine due to the built-in oil lubrication system. A four-stroke engine is typically used for the propulsion of long-life military-type UAVs. The Wankel engine has been redesigned for use in UAV propulsion as a hybrid power generation unit.

Jet engines are used in large UAVs. A jet-type engine's propulsion is produced by releasing liquid fuel combustion products at high velocities, thus inducing thrust that acts as the thrust of the UAV. Rocket engines are powered by liquid or solid fuels. The driving force is obtained by burning fuel. This type of motor has limited use in UAV propulsion because it does not have a mechanism to control the thrust. There is no way to stop the

engine before all fuel is burned. A supercharged jet engine has different stages of rotating blades. Air in the engine enters each stage and each stage compresses the air into stages. The flow path through which air passes gradually decreases in area as it progresses to the next stage. At the end of the compressor, there is a diffuser that slows down the airflow to further increase the static pressure.

An aircraft propeller or a turbofan enclosed in an enclosure is driven by a turboprop or turbofan engine. The compressor is powered in part by the energy produced by the turbine, and the remaining energy is transferred through the reduction gears to the propeller or turbofan. The fundamental distinction between a turbofan and a turbojet engine is that a turbofan uses almost all of its power to drive a propeller, whereas a turbojet uses its exhaust gases to produce tremendous thrust.

The take-off, flight, positioning, and landing of a UAV are often performed with electric propulsion motors. The often-referred-to “copter” UAV can conduct take-off, flight, positioning, and landing procedures with a minimum of three thrust engines. The copter can be placed when the thrust of the electric motors is adjusted and the position and flight path of the UAV are maintained.

A tiny copter UAV can employ a brushed direct current (DC) electric motor as its thrust motor. Due to the existence of airfoil-style wings, it may also power a fixed-wing UAV, eliminating the requirement to generate lifting force. A DC motor can be run on DC current or under pulse width modulation control without the usage of complex electronic speed controller circuitry.

Modern electric motors, known as brushless direct current (BLDC) motors, are frequently utilized in small UAVs that are powered by electricity for all purposes. The key benefits of the motor are:

- The design is more sturdy and compact because brushes, commutators, and slip rings are not used.
- Low rotor inertia results in rapid dynamic reaction; simple, lightweight, and lossless rotor construction yields low inertia and great efficiency.
- High efficiency enables the machine’s structure to be smaller.
- High life cycle occasionally exceeding 30,000 h.
- Due to the fact that the motor windings are a component of the permanent stator, there are no moving electrical components and mechanical commutation.
- High reliability because the only component that is subject to friction force is the bearing.

Permanent magnets spinning around a fixed stator with windings make up a BLDC motor. The electronic speed regulator circuit, which also detects the rotor’s rotational speed and direction, controls the flow of power to the stator windings. High-current pulse width modulation is utilized to regulate motor speed. As a result, the stator windings are activated at varying times while maintaining a consistent frequency.

Internal combustion engines are not used on copter-type UAVs due to the weight, momentum, and lack of mechanical thrust control possibilities of the motor. A mass-produced solution for the use of internal combustion engines in recreational-type copter UAVs has not yet been available. Most recreational copter-type UAVs use electrically driven thrust power plants for propulsion. The only internal combustion engines that could be utilized in copter-type UAVs alongside BLDC electric thrust motors as electric energy generators are probably hybrid internal combustion engines.

1.3. Methods for UAV Detection

The number of approaches to the problem of UAV detection is increasing. Precision, range, operating circumstances, and a host of other factors vary between each method. The most advanced and rapidly evolving techniques for UAV detection are as follows:

- **Examination of the acoustic signal footprint.** An acoustic signal from the UAV’s thrust motors is picked up by a microphone or microphone array that is analyzed and compared to the known UAV’s signal pattern in real time. The UAV is discovered if the signal patterns match [13].

- **Analyzing the optical footprint.** An individual video camera or a camera array is used to record the scene around it. The image data is processed in real-time for the recognition of the signature of the flight-path [14].
- **Examination of heat signatures.** The image of the surroundings is captured using a thermal camera or camera array. The image data is processed in real-time for the recognition of the signature of the flight-path [15].
- **Analysis of a radar signature.** The presence of a UAV's radar signature, which is created when the UAV's body interacts with RF pulses that were emitted by the detecting element. Real-time processing of the UAV's reflected signal for flight path detection. Recently, a concept of a built-in radar in the UAV's structure was proposed [16].
- **Radio transmission.** Real-time reception and analysis of the radio frequency spectrum are performed for modulation, video, telemetry, and control data decoding. Decoding of the well-known communication data packets yields useful information [17].
- **Combined techniques.** Any combination of multiple detection techniques is used for UAV detection in order to improve precision, reliability, stability, location, and range [18].

1.4. Features of UAV Detection Methods

- **Analysis of the acoustic signal characteristics:** Compatible with a variety of other UAV detection techniques. The combination of different techniques effectively improves the accuracy of an optical detection [19]. For example, a microphone array that is easy to deploy for building or perimeter security is presented in [20,21]. These kinds of systems are economical and easy to install in urban places, stadium security, large gatherings, airports, and locations close to noise sources. These kinds of systems are not ideal due to noise interference. The reliability of detection can be affected by rain, wind, and noise. Additionally, there is no capability to track objects.
- **Analysis of optical signatures:** The capability to track objects quickly and precisely. Can be combined with a variety of additional detecting techniques [22]. Possibilities to interact with methods of the artificial intelligence [23,24]. The technology is ineffective in low-light situations, mist, fog, rain, and snow. The problems with low light are not resolved by infrared light. Flying UAVs can be difficult to distinguish from gliders and can cause false alerts [25].
- **Heat signatures:** The study of heat signatures can be combined with a variety of different UAV detection techniques in order to increase the accuracy. However, weather conditions have a significant impact on the accuracy of detection. The thermal signature of birds causes erroneous warnings of UAV detection. As a defense against thermal signature detection, UAVs can utilize thermal shielding and ventilation.
- **Analysis of a radar signature:** This technique allows reaching a high detection range. Passive radar may be used when using another source of sent signals, for example, a TV broadcast signal. Characteristics of digital broadcast signals are successfully used to detect high-altitude UAVs [26]. With the aid of conventional radar devices, huge winged drones can be located [27]. Small drones can be detected using solid-state marine radars in the range of more than half a km [28]. However, UAVs with active RF emitting systems can be set up to fly over detecting zones or close to the surface. Small UAVs with unique construction and materials are difficult to find. It is difficult to identify small birds from UAVs. Due to the impact of radiation on human health and building protection, metropolitan locations are not ideal [29]. The cost of operations and equipment is substantial.
- **Analysis of radio frequency communication signatures:** Software defined radio (SDR) technology is combined with methods of artificial intelligence in order to better accommodate urban reception [30]. High-altitude mobile UAV communication sources can be used for the future development of detection systems with object-tracking capabilities that enable the detection of swarming UAVs [31]. However, early detection methods were only used to detect communications in known frequency ranges. UAV's

control data frequencies are typically low power and can be used on WI-FI, GSM, DVB, or public frequency ranges that are nearly impossible to detect in urban areas. New UAV models were not detected by such systems unless they were uploaded to the system, but only the detection of pre-stored pattern data packets was available. Advances in UAV autopilots have made it possible to complete pre-programmed flight missions in complete radio silence and without RF transmissions.

- **Combined detection methods:** Any known method that is combined by integrating a variety of different sensor types can be used to provide more reliable detection capabilities. Detection reliability is greatly improved when used in conjunction with a voice-assisted video camera array [19,32]. However, the methods require complex coordination between different UAV detection systems of different manufacturers. There is no common interface standard for connecting multiple systems from different manufacturers. Several widely used features in passive and active UAV detection systems are different between manufacturers. As shown in the paper, each UAV detection system manufacturer has different UAV detection capabilities [33]. The system integrates radar, video, audio, and HF UAV detection technology to improve detection reliability. Using multiple types of different UAV detection sensors and technologies minimizes the potential for false alarms in UAV detection and ensures highly flexible system customization options.

1.5. Advantages of UAV Thrust Power Plant Detection

The energy source and the thrust power plant are the two primary components that are obviously necessary for UAV flight operation when the development of small UAV structures is considered historically and from a prospective viewpoint. Numerous additional parts used in UAV operations are rapidly modernizing and becoming obsolete. A tiny UAV that is produced in large quantities often uses an electrically powered BLDC motor as its thrust source. Due to their excellent motor efficiency and dense energy storage capacities, electrically driven UAVs can be built in small sizes and light weights, making them difficult to identify using standard UAV detection techniques.

UAVs already have the ability to fly completely autonomously without the aid of radio communication or GPS. They can be readily programmed to fly over any active radar detection system that emits RF and to carry out the preprogrammed mission in complete radio silence.

UAV manufacturers are competing to increase the maximum payload mass of the UAV with an increase in thrust motor power as a result of the rapidly growing demand for payload and the advances of lightweight battery energy storage technologies. The signature of electromagnetic interference emitted by electrically driven UAVs increases as the thrust power of electric motors increases, requiring increasingly strong switching capabilities for the management of electric motors [34,35]. The increase in the maximum payload or cargo of electrically powered UAVs will also cause a detectable increase in the signature of the electromagnetic interference.

2. Materials and Methods

2.1. Measured Objects

In the performed experiments, two similar-sized multi-rotor UAVs were used for measuring their generated signature of an electromagnetic spectrum. Equipment was chosen according to the possibilities of performing a static flight with the flight stabilization function in use. A similar widely used motor-powered BLDC tool was also selected for comparison with the obtained EM signatures from the multi-rotor UAVs.

First of all, the model of the four brushless electric motor-powered Eachine FPV Tyro 109 was used in the experiments. The drone has a built-in flight controller, capable of performing flight stabilization functions. After the flight controller was calibrated for the correct horizontal position, any external force applied to the drone body on any of the three rotation axes makes the engines interact individually in order to obtain the

position it was calibrated for. The stabilization function results in an independent change of the thrust engine's acceleration and rotation speed. The unique electromagnetic field change influenced by the change of power of brushless motors results in an electromagnetic spectrum signature of the drone.

The second drone that was used in the experiments is the well-known model of the Mavic 2 Enterprise from the DJI company. The drone is powered by four small-size brushless electric motors. The performed measurements and used experimental techniques were the same as with the Eachine drone.

The electromagnetic spectrum of the Dewalt DCF809 270 brushless motor powered impact driver is also received and recorded for the evaluation of the experimental results from drones. This is the most common tool that is powered by the closest size brushless electric motor (BLDC) and has the ability to accelerate fast. Additionally, the electric impact driver has the unique load characteristics of an electric engine when the hammer force is in action. The resulted load during hammer action load on the brushless engine has a unique signature in the received electromagnetic spectrum.

All received signatures of the electromagnetic spectrum were recorded for evaluation and comparison.

2.2. Measurement Equipment

The antenna is the most important device of the overall engine signature detection systems. The antenna must have the following characteristics. First of all, it should be selective. There should be a possibility to receive the signal from 1 to 100 kHz.

The resonant frequency range of the antenna should be from 1 kHz to 100 kHz, because different manufacturers use different motors that have their own programmed frequency of the pulse width modulation. Two drones and an electric-powered impact driver were used during experiments, all of which were powered by a similar type, size, and acceleration-capable brushless electric motors that have their own unique signatures on the electromagnetic spectrum.

The ferrite rod of the widely used radio magnetic antenna has standard physical dimensions: diameter 10 mm, length 200 mm, and ferrite type 600NN. The widely available standard ferrite rod type 600NN ($\Phi 600$) has a maximum working frequency of 4 MHz, which satisfies the condition of signal reception at the interval of 1–100 kHz. The ferrite rod also satisfies physical conditions (diameter—10 mm, length—200 mm) for implementation of stepless induction change using the precision linear motor actuator. The coil's parameters were selected according to the specification of the ferrite rod, which satisfies the stepless reception frequency range from 1 kHz to 100 kHz. The antenna setup for the experiment was chosen according to the future prospects of the development of the multi-rod tunable antenna. Several rods with the same physical dimensions and characteristics will be used in order to increase the sensitivity of the reception of the signature from the electromagnetic spectrum and in order to realize the capability of the direction finding.

Selectivity is a must-have property in this kind of system because it is necessary to investigate not only the main harmonics falling into this interval but also additional harmonics. Additional harmonics can be useful in order to avoid environmental interference when environmental noise does not allow unambiguous identification of the drone from the main harmonic. Additionally, the property of selectivity allows isolating and analyzing several harmonics separately. This functionality allows verifying the assumption that the drone has been detected more accurately.

The uniqueness of the proposed antenna is that it is a magnetic antenna that is insensitive to the electrical component of the signal. This is its advantage in comparison with electromagnetic antenna, in which the electrical component adds interference that interferes with detection. There could be many different sources of environmental disturbances. For example, the sources of interference in the city could be outdoor lighting, ultrasonic sensors, power lines of trolleybuses, and others.

Another outstanding advantage of such an antenna is the stepless change of resonant frequency while maintaining maximum interference with ambient noises and high selectivity.

The proposed model of the antenna is presented in Figure 2. The resonant frequency of the antenna could be changed by varying the inductance and/or capacitance in the antenna matching circuit. There was no option to apply the variable capacitor of large capacity which is required in such type of antennas. Therefore, this antenna was realized by varying the inductance. The ferrite rod and the motorized actuator that were used affect the capacitance and change the resonant frequency of the proposed magnetic antenna.

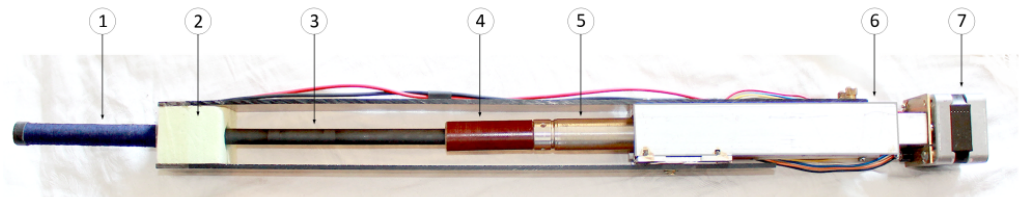


Figure 2. Precision tunable variable inductance magnetic antenna. 1—antenna coil with cooper windings; 2—antenna coil holder; 3—linear motion actuated ferrite rod; 4—insulating textolite insert; 5—shaft of the precision linear actuator; 6—body of the precision linear actuator; 7—step motor of the linear actuator. The dimensions of the proposed and manufactured antenna are coil length—100 mm; coil diameter—13 mm; ferrite rod diameter—10 mm; ferrite rod length—200 mm; insulator length—50 mm; overall system length of the magnetic antenna—600 mm.

Such a tunable antenna allows scanning the environment (electromagnetic spectrum) and detecting the trace of the motors of drones in the spectrogram. The trace of the motor in the spectrogram could be additionally verified by analyzing the higher harmonics of the spectrum.

The dimensions of the antenna are determined by several factors. In order to achieve higher sensitivity, it is necessary to manufacture a longer and wider ferrite rod. Therefore, larger dimensions are aspirational. On the other hand, it was necessary to stick to the maximum available size of the ferrite rod during the production of the prototype. Consequently, the variable inductance of the variable magnetic antenna could vary in the range of 5–258 mH.

The experimental studies with the proposed tunable antenna were carried out by changing the distance of the motor from the antenna in the range of up to 4 m using an SDR receiver. The signals can be detected at a distance of 25 m or more by using the short wave receiver.

Additional equipment was also used during measurement in order to collect the data from the antenna. First of all, the software defined radio receiver USRP 2920 from National Instruments was used. The reception range of the particular model is DC–30 MHz. The local ethernet communication line was used for data transmission. Additionally, the advanced software-defined radio Airspy Discovery +HF receiver was used. The reception range of the following SDR is 500 Hz–31 MHz. The data transmission is implemented using a USB interface. The SDR Console version 3.1, running on Windows 10 PRO operating system was used for both above-mentioned SDRs.

2.3. Experimental Setup

First of all, the multi-rotor UAV is permanently fixed on a holder during the experiments. The holder is implemented using the tripod interconnecting ball joint (see Figure 3). This kind of construction of the presented holder allows the free rotation of the UAV in three axes representing the yaw, pitch, and roll of the UAV during normal flight. The horizontal position of the UAV is obtained by using a counterweight that is connected to the tripod ball joint. When all the UAV's thrust engines are turned off, the counterweight stabilizes the UAV in a perfect horizontal plane, thus making it possible to apply any force

direction that is produced by the UAV's thrust engines or any external force. The altitude of the UAV is fixed and stays the same during the experiment.

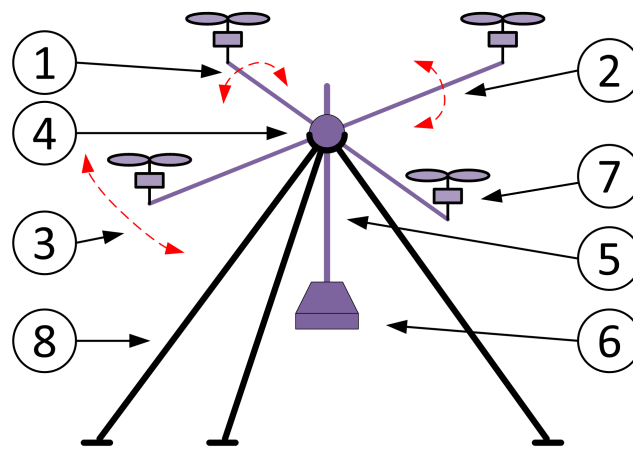


Figure 3. The experimental test bench of the tripod interconnecting ball joint holder: 1—roll axis of the UAV fixture; 2—pitch axis of the UAV fixture; 3—yaw axis of the UAV fixture; 4—the UAV's fixture connecting ball joint; 5—the UAV's fixture horizontal stabilizer connecting rod; 6—the UAV's fixture horizontal stabilizer counterweight; 7—UAV's thrust engine; 8—holder.

A precision tunable variable inductance magnetic antenna is placed 1 to 5 m from the UAV. The antenna is connected to the SDR receiver, which sends data to the personal computer with dedicated software. Initially, the ES of the surrounding was recorded and examined in order to evaluate the presence of any artifacts before powering on the UAV thrust engines. The electric thrust motors of the UAV started to spin at a minimal speed. The control of the motors was established using the remote controller of the UAV. The signature of the ES was observed and recorded.

Next, the thrust engines are powered up to 40% of the full throttle with the stabilization function activated while the UAV stays permanently fixed to the holder. The force to the UAV's body is applied in a such way that the stabilization on any of yaw, pitch, and roll axes is present and visible as an ES signature. To confirm that the ES signature is not an artifact, force to the UAV's body is applied in a repetitive way, which is also represented in the recorded UAV's ES signature. The connected counterweight system was used in the experiment as a pendulum for a repetitive external force generation to any of the UAV's axes except yaw.

Any small applied force to the UAV's body leaves a proportional frequency change as the ES signature during the stabilization mode. This kind of experimental setup is an alternative to the UAV's natural free-flight conditions in order to simulate any wind gust, take off, landing, yaw, pitch, and roll axis movements.

The physical experiments are based on collecting data on the operating modes of different engines from different drones (see Figure 4).

Several engines were used as a source of investigation. First of all the engine from the DEWALT DCF809 impact drive was used in the investigation, because its spectrum is similar to the spectrums of engines from drones. The second engine used was from a DJI MAVIC 2 Enterprise drone. The last engine was from the ACHINE TYRO 109 multi-rotor drone.

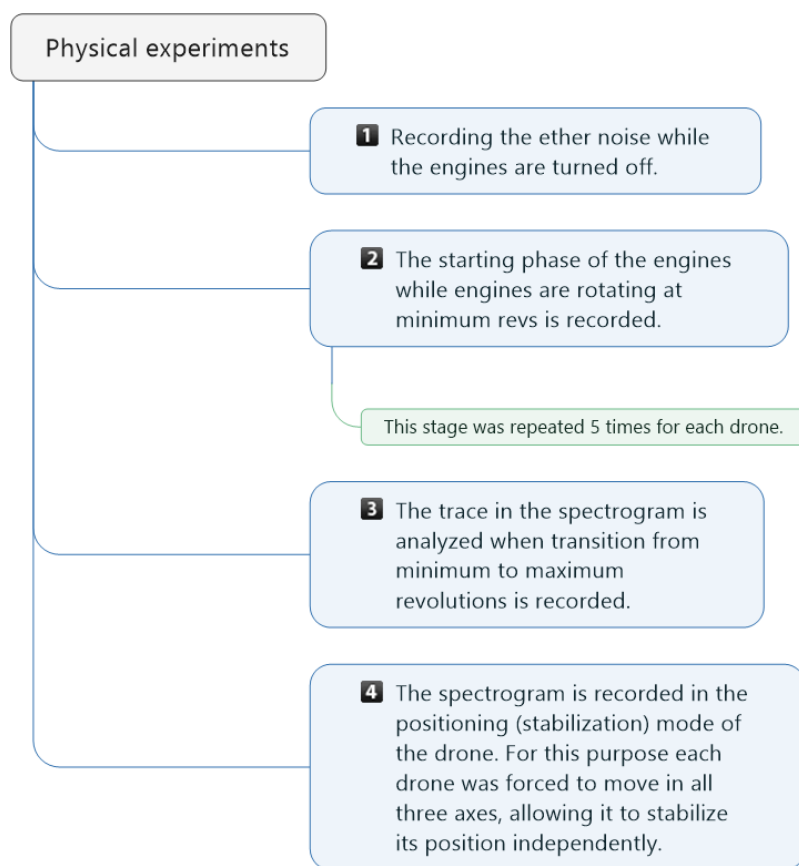


Figure 4. Performance of the physical experiments.

3. Results and Discussion

The physical experiments were conducted with three engines from three different sources. First of all, two similar-sized multi-rotor UAVs were used for measuring their generated signature on an electromagnetic spectrum. The equipment was chosen according to the possibilities of performing a static flight with the flight stabilization function in use. The first engine was from a DJI MAVIC 2 Enterprise drone and the second engine was from an ACHINE TYRO 109 multi-rotor UAV drone, respectively. A similar BLDC motor from the widely used DEWALT DCF809 impact drive was selected for the comparison of the obtained ES signatures, which were generated by the engines of multi-rotor UAVs.

From Figures 5–10, one can see that after applying the tunable repositioning of the ferrite rod it is possible to achieve:

- Smooth (continuous) variation of the resonant frequency.
- It is possible to detect both the first and other higher harmonics of the electromagnetic spectrum which are emitted by engines of the drone.
- Environmental disturbances are eliminated during measurements. The system is not sensitive to environmental disturbances.

There were 100 attempts made with every selected device in order to get the electromagnetic spectrograms. Overall, there were 300 attempts. The three summarizing spectrograms are presented for discussion. The aim of the work was to confirm the concept that the designed and manufactured tunable magnetic antenna allows identifying the appearance of the drone in the research area. Additionally, the magnetic antenna allows identifying different operation modes of the engines of the investigated drones.

First of all, the 30 s window of the spectrogram of the engine from the Eachine Tyro multi-rotor UAV is presented in Figure 5. The visible essential areas of the spectrogram are: 1—the UAV’s thrust motors are turned off; 2—the UAV’s thrust motors are spinning

at minimal idle rotation speed; 3—the UAV's thrust motors are spinning from 40% to 30% of the full power; 4—the UAV's thrust motors are spinning at 40% of full power while forced repetitive body destabilization movements in the pitch, yaw, and spin axes are performed. Each forced movement of the UAV is generating a unique signature in an electromagnetic spectrum which is proportional to the frequency shift of the signal. 5—the UAV's thrust motors are spinning at 50% of full power. Equal repetitive forced body destabilization movements in the pitch axis are performed. Each forced movement is generating a proportional signal's frequency shift in an electromagnetic spectrum. 6—the UAV's thrust motors are spinning at the minimal idle rotation speed.

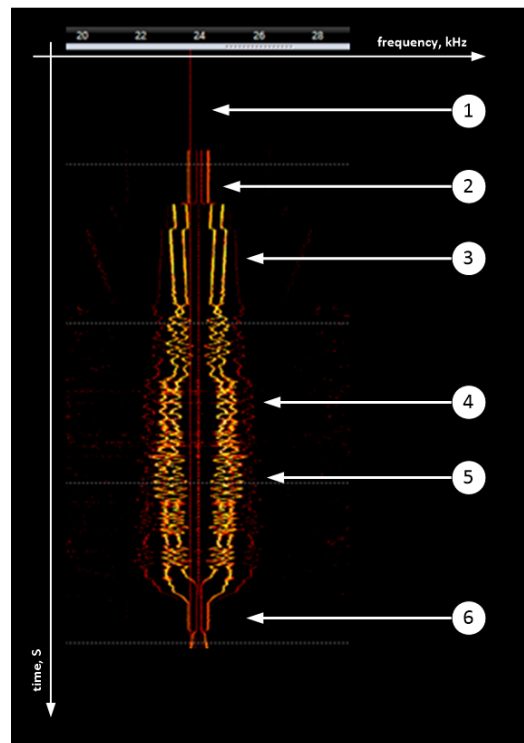


Figure 5. Recorded signature of a 24 kHz electromagnetic spectrogram, generated by the thrust engines of the multi-rotor Eachine Tyro UAV.

According to the results from the spectrogram, it is visible that the appearance of the working engines of the drones is clearly visible in the spectrogram. The actual mode of operation of the engines of the drone can be also identified by using the spectrum of the obtained signal to the magnetic antenna. The level of the amplitude of the spectrum and the distribution of energy at different frequencies will be different in the different modes of operation.

For example, the spectrum of obtained signals to the magnetic antenna from all four engines while working in the 50% power of the engines (fifth mode) is presented in Figure 6. The energy of the signal is more concentrated in the lower frequencies.

On the other hand, while the UAV's thrust motors are spinning at a minimal idle rotation speed, peaks of amplitudes and the root mean square (RMS) will have the lower values. Additionally, the energy in percentages will be more spread out in higher frequencies (see Figure 7).

A similar situation is obtained in the spectrograms of the engines from the DJI MAVIC 2 Enterprise drone (see Figure 8).

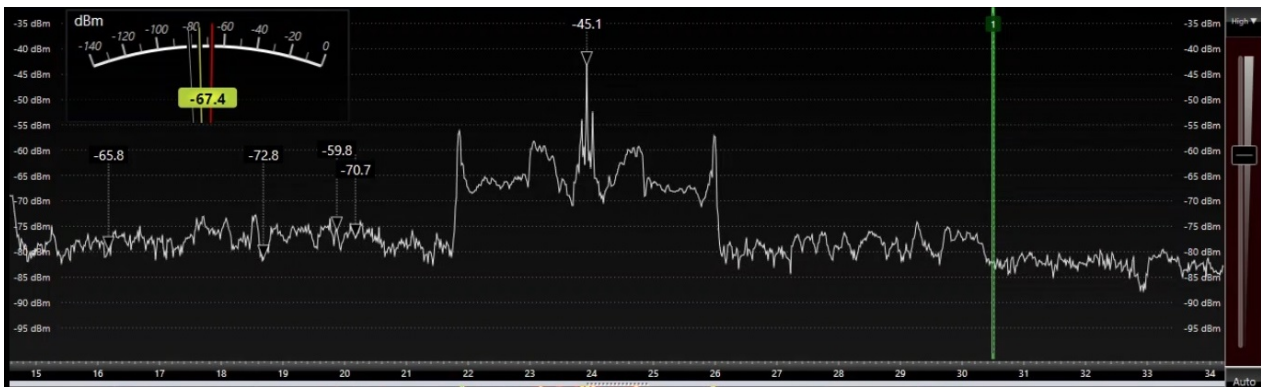


Figure 6. Spectrum of the multi-rotor Eachine Tyro UAV at the fifth operating mode while engines work at 50% of its maximum power.

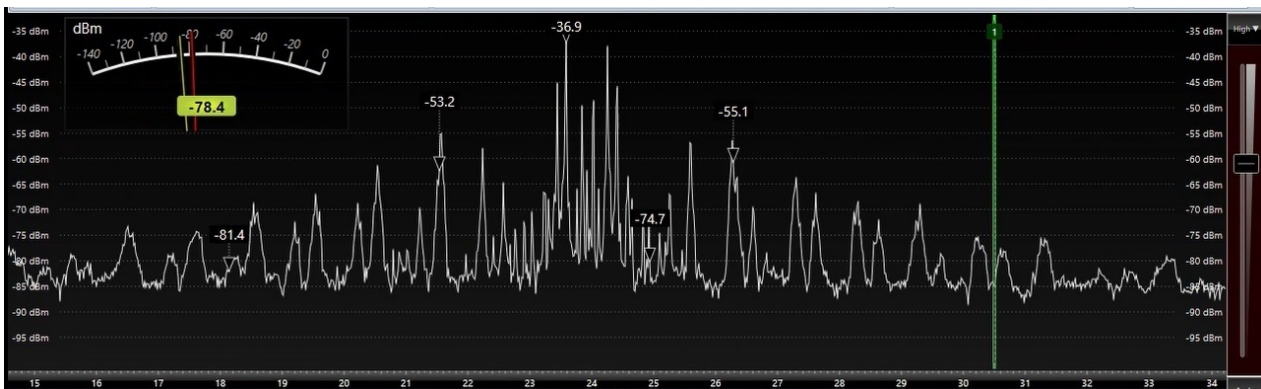


Figure 7. Spectrum of the multi-rotor Eachine Tyro UAV when the thrust motors are spinning at the minimal idle rotation speed.

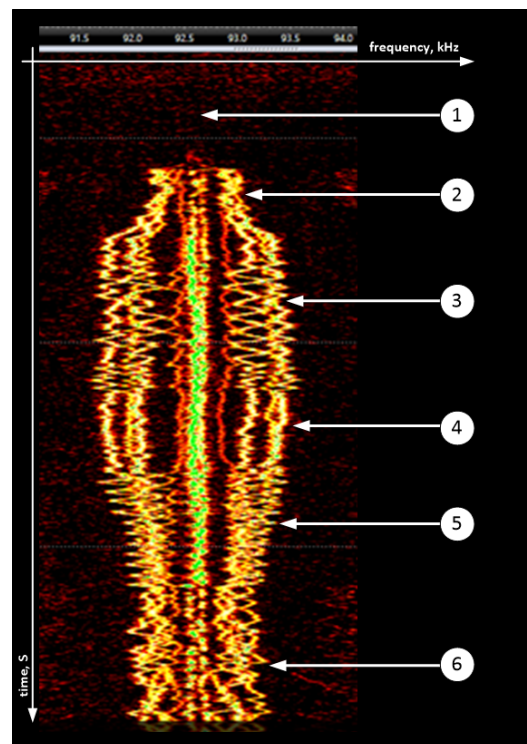


Figure 8. Recorded signature of a 92 kHz electromagnetic spectrogram, generated by the thrust engines of the multi-rotor DJI Mavic 2 Enterprise UAV.

Again, the 30 s window of the spectrogram is presented in Figure 8. The essential areas of the spectrogram are: 1—the UAV's thrust motors are turned off; 2—the UAV's thrust motors are spinning at a minimal idle rotation speed; 3—the UAV's thrust motors are turning at 40% of the full power. Forced, equal and repetitive destabilization movements in the pitch axis are applied to the body of the UAV. Each forced movement is generating a proportional frequency shift of the signal in an electromagnetic spectrum. 4—the UAV's thrust motors are spinning at 80% of full power, takeoff static motor thrust is generated in stabilization mode; 5—the UAV's thrust motors are turning at 30% of full power, equal repetitive forced destabilization movements in the pitch axis are performed. Each forced movement is generating a proportional signal's frequency shift in an electromagnetic spectrum. 6—the UAV's thrust motors are turning at 30% of full power. Forced repetitive body destabilization movements in the pitch, yaw, and spin axes are performed.

The last spectrogram is presented of the motor that is not from the drone, but from the DEWALT DCF809 impact driver (see Figure 9). The time window of the spectrogram is 30 s. The spectrogram of the Dewalt DCF809 impact driver has five essential working modes: 1—the BLDC impact driver motor in slow speed impact mode under the load, hammer in action; 2—the BLDC impact driver motor driving a bolt without impact hammer operation; 3—the BLDC impact driver motor under load condition, with pretension of the hammer spring; 4—the BLDC impact driver motor under load with the hammer in action; 5—the BLDC impact driver motor switched off.

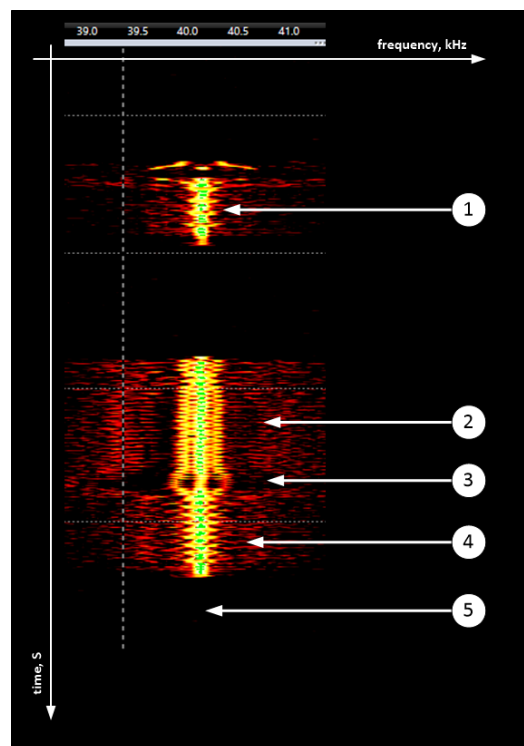


Figure 9. Recorded signature of a 40 kHz electromagnetic spectrogram, generated by the single BLDC motor of the Dewalt impact driver.

The physical experiments have shown that every set of engines of the drone could be recognized using the proposed and investigated tunable magnetic antenna. For example, the DJI drones have a specific signature in the spectrogram obtained during engine start-up, which allows the drone type/manufacturer to be identified from the spectrogram. All the transitions from minimum to maximum revolutions of the engines were visible in the spectrograms with their unique signatures. A clearly visible signature in the spectrogram was obtained in the fundamental and other higher harmonics of the spectrum while measuring the drone signature in the spectrogram positioning (stabilization) mode.

The higher harmonics could be investigated by shifting the resonant frequency of the antenna. For example, a precision tunable variable inductance magnetic antenna shifted the frequency from 23 kHz to 46 kHz and back to 23 kHz (see Figure 10). As it is seen from the recorded spectrum, the amplitude of the second harmonic increased and became visible for recognition. Comparing different harmonics of the same signal and continuous tracking of the ES signature enables new capabilities of AI-powered UAV detection systems.

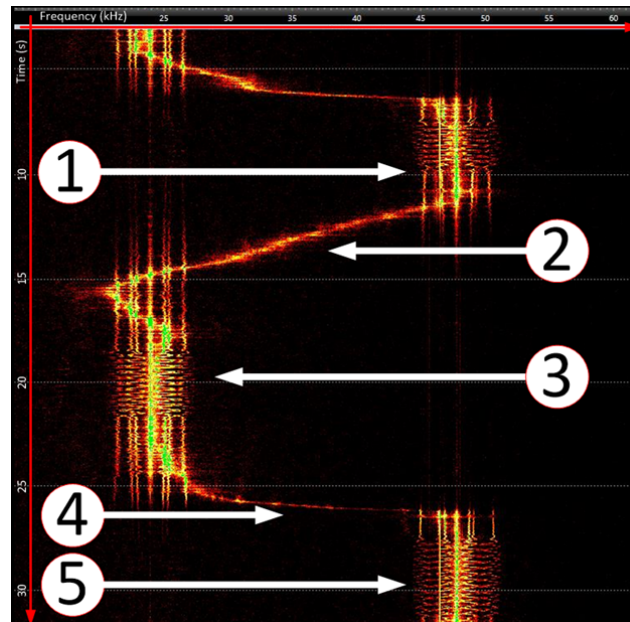


Figure 10. Spectrogram of antenna with shifted frequency from 23 kHz to 46 kHz and back to 23 kHz, when 1—received UAV EM spectrum signature of the second harmonic; 2—stepless transition of magnetic antenna resonant frequency to the first harmonic of UAV EM spectrum signature; 3—received UAV EM spectrum signature of the first harmonic; 4—stepless transition of magnetic antenna resonant frequency to the second harmonic of UAV EM spectrum signature; 5—received UAV EM spectrum signature of the second harmonic.

A precision tunable variable inductance magnetic antenna can be used together with the AI systems for more reliable ES signature detection and recognition. The advantage of the antenna is that it can track the movement of the ES signature in ES continuously or jump to any other frequency with precalculated harmonics for signature evaluation or comparison.

In the case of a situation when the investigated harmonic at the particular frequency of the UAV's ES signature is with high disturbances, variable inductance magnetic antenna can instantaneously change reception frequency to other harmonics for signature reception and comparison. According to the obtained spectrograms from different engines, it is possible to summarize that:

- ES signatures of electrically powered multi-rotor UAVs are received, recorded, and analyzed.
- ES signatures of Dewalt impact driver are received, recorded, and analyzed.
- There are enough data to conclude that ES signatures of engines from different drones and ES signature of engine from impact driver generates completely different ES signatures.
- A precision tunable variable inductance magnetic antenna can be used to detect the first harmonic of the UAV's ES signature and then retune to the second or any other present harmonics.
- An antenna capable of tuning harmonics can increase the effectiveness of signature detection algorithms by checking ES signatures between the different harmonics of the same UAV.

- Each forced movement of the UAV generates a unique signature in an electromagnetic spectrum that is proportional to the frequency shift of the signal.

For example, the comparison of the ES signature of the Eachine Tyro drone in the spectrogram with all five harmonics in the 0–120 kHz frequency range are presented in Figure 11a. Overall, there are five harmonics at 24, 48, 72, 96, and 120 kHz frequencies, respectively. In the case of the DJI drone, there are three harmonics (see Figure 11b). The width of the different harmonics in the spectrogram of the Dewalt impact driver are compared in Figure 11c.

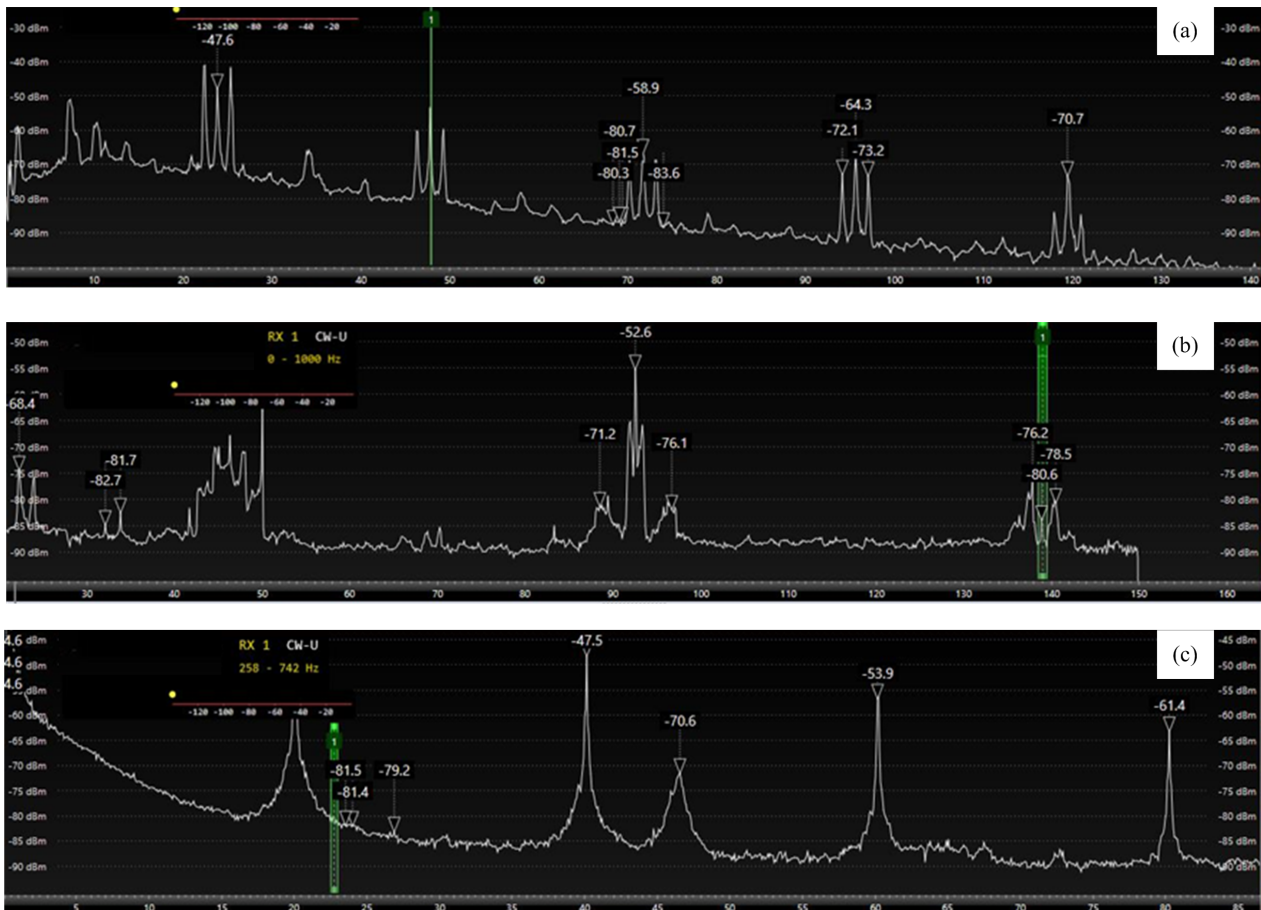


Figure 11. Spectrograms of engines with all visible harmonics and their widths in the 0–120 kHz frequency range: (a)—Eachine Tyro drone; (b)—DJI drone; (c)—Dewalt impact driver.

A more detailed comparison of spectrograms of the main frequencies of the harmonics of the UAVs is presented in Tables 1–3.

Table 1. Main frequencies of the harmonics of the Eachine Tyro drone’s spectrogram.

Harmonics	1	2	3	4	5
The lower frequencies of the harmonic signature, Hz	21,806	45,548	69,677	93,419	117,290
The upper frequencies of the harmonic signature, Hz	26,064	49,806	73,806	97,815	121,548
The width of the harmonic signature, Hz	4258	4258	4129	4396	4258
The center frequencies of the harmonic signature, Hz	24,000	47,870	71,612	95,612	119,612
The amplitude of center frequency, dBm	−47.6	−51.2	−58.9	−64.3	−70.7

Table 2. Main frequencies of the harmonics of the DJI drone’s spectrogram.

Harmonics	1	2	3
The lower frequencies of the harmonic signature, Hz	42,468	88,793	135,465
The upper frequencies of the harmonic signature, Hz	49,977	96,533	142,859
The width of the harmonic signature, Hz	7509	7740	7394
The center frequencies of the harmonic signature, Hz	46,280	92,575	13,8931
The amplitude of center frequency, dBm	−66.1	−52.6	−80.6

Table 3. Main frequencies of the harmonics of the Dewalt driver’s spectrogram.

Harmonics	1	2	3	4
The lower frequencies of the harmonic signature, Hz	19,392	39,413	59,612	79,733
The upper frequencies of the harmonic signature, Hz	20,791	40,878	60,998	81,198
The width of the harmonic signature, Hz	1399	1465	1386	1465
The center frequencies of the harmonic signature, Hz	20,090	40,110	60,270	80,221
The amplitude of center frequency, dBm	−41.6	−47.5	−53.9	−61.4

The more detailed comparison of spectrograms shows that the mean width of the harmonic signature is 4259.8 Hz. The third harmonic has the narrowest width, which is equal to 4129 Hz and the fourth harmonic has the widest width, which is equal to 4396 Hz. The highest center frequency of the harmonic signature could be received in the case of the fifth harmonic—119,612 Hz and the lowest 24,000 Hz at the first harmonic (see Table 1).

The three harmonics could be received in the case of the DJI drone. The mean width of the harmonic signature is 7547.6 Hz. The width of the harmonic signatures varies from 7394 Hz to 7740 Hz. The center frequencies of the harmonic signature vary from 46,280 Hz to 138,931 Hz in all three harmonics (see Table 2).

The narrowest width of the harmonic signature is received in the case of the Dewalt driver, the lowest width of the harmonic signature is 1386 Hz in the case of the third harmonic. Additionally, we detected only four harmonics (see Table 3). The center frequencies of the harmonic signature vary from 20,090 Hz to 80,221 Hz.

The analysis of the multi-rotor UAVs shows that the center frequencies of the harmonic signature vary from 24,000 Hz to 13,8931 Hz. The width of the harmonic signature varies from 4129 Hz to 7394 Hz compared with the width of the harmonic signature of the Dewalt driver. Therefore, the center frequency of the harmonic signature of the first harmonic of the Dewalt driver is pushed to the lower side of the frequencies compared with other BLDCmotors.

4. Conclusions

In this study, a hypothesis was validated that, by measuring the spectrum of engine control signals, it is possible to detect UAV-specific traces in the spectrogram. In the Introduction section, it was shown that electromagnetic interference signatures are expected to increase, due to the emergence of electric motors.

Thus, in this study, we showed that it is possible to detect a signature of an electromagnetic spectrum of multi-rotor UAVs. The interference frequency range is expected to be from 1 to 100 kHz. For this task, a precision tunable variable inductance magnetic antenna design was proposed.

The resonant frequency of the designed tunable antenna is changed by varying the inductance using a motorized actuator. The obtained results show a change in the spectrogram based on the thrust of the engine and the different types of UAVs.

Author Contributions: Conceptualization, T.J. and V.U.; methodology, A.S., V.A. and D.P.; formal analysis, A.K., T.S. and D.P. investigation, T.J.; writing—original draft preparation, V.A. and T.S.; writing—review and editing, D.P. and A.K.; visualization, T.J.; supervision, A.S. and D.P.; funding acquisition, A.S. All authors have read and agreed to the published version of the manuscript.

Funding: This research received no external funding.

Institutional Review Board Statement: Not applicable.

Informed Consent Statement: Not applicable.

Data Availability Statement: Data sharing not applicable.

Acknowledgments: The authors would like to thank the editors and reviewers for many constructive suggestions and comments that helped improve the quality of the paper.

Conflicts of Interest: The authors declare no conflict of interest.

References

1. Cieślak, E. Unmanned Aircraft Systems: Challenges to Air Defense. *Saf. Def.* **2021**, *1*, 72–83.
2. Pyrgies, J. The UAVs threat to airport security: Risk analysis and mitigation. *J. Airl. Airt. Manag.* **2019**, *9*, 63–96. [[CrossRef](#)]
3. Chaari, M.Z.; Al-Maadeed, S. The game of drones/weapons makers' war on drones. In *Unmanned Aerial Systems*; Elsevier: Amsterdam, The Netherlands, 2021; pp. 465–493.
4. Freedman, L. Why War Fails: Russia's Invasion of Ukraine and the Limits of Military Power. *Foreign Aff.* **2022**, *101*, 10.
5. Russell, L.; Goubran, R.; Kwamena, F. Emerging urban challenge: RPAS/UAVs in cities. In Proceedings of the 2019 15th International Conference on Distributed Computing in Sensor Systems (DCOSS), Santorini Island, Greece, 29–31 May 2019; pp. 546–553.
6. Christensen, C.; Salmon, J. An agent-based modeling approach for simulating the impact of small unmanned aircraft systems on future battlefields. *J. Def. Model. Simul.* **2022**, *19*, 481–500. [[CrossRef](#)]
7. Chin, J.; Escribà-Folch, A.; Song, W.; Wright, J. Reshaping the Threat Environment: Personalism, Coups, and Assassinations. *Comp. Political Stud.* **2022**, *55*, 657–687. [[CrossRef](#)]
8. Yaacoub, J.P.; Noura, H.; Salman, O.; Chehab, A. Security analysis of drones systems: Attacks, limitations, and recommendations. *Internet Things* **2020**, *11*, 100218. [[CrossRef](#)]
9. Madanayake, A.; De Silva, H.; Glickstein, J.; Mandal, S. Extremely-Low Frequency (ELF) Radio Sensing of Unmanned Aerial Systems. In Proceedings of the 2022 United States National Committee of URSI National Radio Science Meeting (USNC-URSI NRSMS), Boulder, CO, USA, 4–8 January 2022; pp. 115–116.
10. Blažek, J.; Lipovský, P.; Heško, F.; Repčík, D. Electromagnetic image of small UAV in very low frequency range. *J. Electr. Eng.* **2018**, *69*, 438–441. [[CrossRef](#)]
11. Novotňák, J.; Oravec, M.; Híj, J.; Jurč, D. Slip Control by Identifying the Magnetic Field of the Elements of an Asynchronous Motor. In Proceedings of the 2021 IEEE 19th World Symposium on Applied Machine Intelligence and Informatics (SAMII), Herľany, Slovakia, 21–23 January 2021; pp. 000273–000278.
12. Blažek, J. Leakage magnetic fields of the electric BLDC motors of small UAV. *J. Electr. Eng.* **2015**, *66*, 14–17.
13. Kim, J.; Park, C.; Ahn, J.; Ko, Y.; Park, J.; Gallagher, J.C. Real-time UAV sound detection and analysis system. In Proceedings of the 2017 IEEE Sensors Applications Symposium (SAS), Glassboro, NJ, USA, 13–15 March 2017; pp. 1–5.
14. Rzucidło, P.; Jaromi, G.; Kapuściński, T.; Kordos, D.; Rogalski, T.; Szczerba, P. In-Flight Tests of Intruder Detection Vision System. *Sensors* **2021**, *21*, 7360. [[CrossRef](#)]
15. Beaver, J.T.; Baldwin, R.W.; Messenger, M.; Newbolt, C.H.; Ditchkoff, S.S.; Silman, M.R. Evaluating the use of drones equipped with thermal sensors as an effective method for estimating wildlife. *Wildl. Soc. Bull.* **2020**, *44*, 434–443. [[CrossRef](#)]
16. Rudys, S.; Laučys, A.; Ragulis, P.; Aleksiejūnas, R.; Stankevičius, K.; Kinka, M.; Razgūnas, M.; Bručas, D.; Udris, D.; Pomarnacki, R. Hostile UAV Detection and Neutralization Using a UAV System. *Drones* **2022**, *6*, 250. [[CrossRef](#)]
17. Farlik, J.; Kratky, M.; Casar, J.; Stary, V. Multispectral detection of commercial unmanned aerial vehicles. *Sensors* **2019**, *19*, 1517. [[CrossRef](#)] [[PubMed](#)]
18. Chamola, V.; Kotesch, P.; Agarwal, A.; Gupta, N.; Guizani, M.; A comprehensive review of unmanned aerial vehicle attacks and neutralization techniques. *Ad. Hoc. Netw.* **2021**, *111*, 102324. [[CrossRef](#)] [[PubMed](#)]
19. Liu, H.; Wei, Z.; Chen, Y.; Pan, J.; Lin, L.; Ren, Y. Drone detection based on an audio-assisted camera array. In Proceedings of the 2017 IEEE Third International Conference on Multimedia Big Data (BigMM), Laguna Hills, CA, USA, 19–21 April 2017; pp. 402–406.
20. Pechan, T.; Sescu, A. Experimental study of noise emitted by propeller's surface imperfections. *Appl. Acoust.* **2015**, *92*, 12–17. [[CrossRef](#)]
21. Sinibaldi, G.; Marino, L. Experimental analysis on the noise of propellers for small UAV. *Appl. Acoust.* **2013**, *74*, 79–88. [[CrossRef](#)]

22. Teixidó, P.; Gómez-Galán, J.A.; Caballero, R.; Pérez-Grau, F.J.; Hinojo-Montero, J.M.; Muñoz-Chavero, F.; Aponte, J. Secured Perimeter with Electromagnetic Detection and Tracking with Drone Embedded and Static Cameras. *Sensors* **2021**, *21*, 7379. [[CrossRef](#)]
23. Chen, Y.; Aggarwal, P.; Choi, J.; Kuo, C.C.J. A deep learning approach to drone monitoring. In Proceedings of the 2017 Asia-Pacific Signal and Information Processing Association Annual Summit and Conference (APSIPA ASC), Kuala Lumpur, Malaysia, 12–15 December 2017; pp. 686–691.
24. Liu, H.; Fan, K.; Ouyang, Q.; Li, N. Real-time small drones detection based on pruned yolov4. *Sensors* **2021**, *21*, 3374. [[CrossRef](#)]
25. Unlu, E.; Zenou, E.; Riviere, N.; Dupouy, P.E. Deep learning-based strategies for the detection and tracking of drones using several cameras. *IPSIJ Trans. Comput. Vis. Appl.* **2019**, *11*, 7. [[CrossRef](#)]
26. Fang, G.; Yi, J.; Wan, X.; Liu, Y.; Ke, H. Experimental research of multistatic passive radar with a single antenna for drone detection. *IEEE Access* **2018**, *6*, 33542–33551. [[CrossRef](#)]
27. Eriksson, N. Conceptual Study of a Future Drone Detection System-Countering a Threat Posed by a Disruptive Technology. Master's Thesis, Department of Industrial and Materials Science, Chalmers University of Technology, Gothenburg, Sweden, 2018.
28. Rudys, S.; Ragulis, P.; Laučys, A.; Bručas, D.; Pomarnacki, R.; Plonis, D. Investigation of UAV Detection by Different Solid-State Marine Radars. *Electronics* **2022**, *11*, 2502. [[CrossRef](#)]
29. Hinojosa, I.; Letertre, T.; Mazières, V. UAV detection with K band embedded FMCW radar. In Proceedings of the 2017 Mediterranean Microwave Symposium (MMS), Marseille, France, 28–30 November 2017; pp. 1–4.
30. Chiper, F.L.; Martian, A.; Vlădeanu, C.; Marghescu, I.; Craciunescu, R.; Fratu, O. Drone Detection and Defense Systems: Survey and a Software-Defined Radio-Based Solution. *Sensors* **2022**, *22*, 1453. [[CrossRef](#)] [[PubMed](#)]
31. Ezuma, M.; Erden, F.; Anjinappa, C.K.; Ozdemir, O.; Guvenc, I. Micro-UAV detection and classification from RF fingerprints using machine learning techniques. In Proceedings of the 2019 IEEE Aerospace Conference, Big Sky, MT, USA, 2–9 March 2019; pp. 1–13.
32. Taha, B.; Shoufan, A. Machine learning-based drone detection and classification: State-of-the-art in research. *IEEE Access* **2019**, *7*, 138669–138682. [[CrossRef](#)]
33. Jačionis, T. Modern methods for detection of unmanned aerial vehicles. *Moksl.—Liet. Ateitis/Sci.—Future Lith.* **2020**, *12*, 1–6. [[CrossRef](#)]
34. Blažek, J. Modelling and simulation of the possible em radiation of the power supply towards the synchronized and bldc motors. *J. Electr. Eng.* **2015**, *66*, 18–21.
35. Lipovský, P.; Heško, F.; Moucha, V.; Bažek, J. Possible detection of multirotor UAVs based on disturbances in magnetic field. In Proceedings of the 2018 XIII International Scientific Conference-New Trends in Aviation Development (NTAD), Kosice, Slovakia, 30–31 August 2018; pp. 91–95.